Role of surface latent heat flux in shallow cloud transitions: A mechanism-denial LES study

Youtong Zheng, Haipeng Zhang, and Zhanqing Li

Affiliations:

Earth System Science Interdisciplinary Center, University of Maryland, College Park, Maryland, 20742, USA.

Corresponding author: Youtong Zheng, Earth System Science Interdisciplinary Center, University of Maryland, College Park, Maryland, 20742, USA, zhengyoutong@gmail.com

Key points:

- A mechanism-denial LES study confirms the key role of latent heat flux (LHF) in driving the stratocumulus-to-cumulus transition (SCT).
- Under weak capping inversions, the boundary layer can decouple without the need for LHF to increase, but the decoupled state cannot sustain.
- Larger LHF can shorten the lifetime of the stratocumulus deck due to the enhanced entrainment drying by cumulus penetration.

Abstract

Surface latent heat flux (LHF) has been deemed as the determinant driver of the stratocumulus-to-cumulus transition (SCT). The distinct signature of the LHF in driving the SCT, however, has not been found in observations. This motivates us to ask: how determinant the LHF is to SCT? To answer it, we conduct large-eddy simulations in a Lagrangian setup in which the sea-surface temperature increases over time to mimic a low-level cold air advection. To isolate the role of LHF, we conduct a mechanism-denial experiment in which the LHF adjustment is turned off to evaluate the response of SCT. The simulations confirm the indispensable roles of LHF in sustaining (although not initiating) the boundary layer decoupling (first stage of SCT) and driving the cloud regime transition (second stage of SCT). Specifically, we found that decoupling can happen without the need for LHF to increase as long as the capping inversion is weak enough to ensure high entrainment efficiency. The decoupled state, however, cannot sustain without the help of LHF adjustment, leading to the recoupling of the boundary layer. In the coupled boundary layer, the stratocumulus sheet thins over time due to the lack of moisture supply, eventually leading to a cloud-free boundary layer. Interestingly, the stratocumulus sheet sustains longer without LHF adjustment. The mechanisms underlying the findings are explained from the perspectives of cloud-layer budgets of energy (first stage) and liquid water path (second stage). Lastly, we develop a new model diagnostic that offers a physically robust conceptualization of boundary layer decoupling.

Plain Language Summary

A climatologically important but poorly understood phenomenon about the stratocumulus (low-lying blanket-like clouds) is its tendency to transit to cumulus clouds (scattered cauliflower-like clouds) as the underlying sea surface warms, called the stratocumulus-to-cumulus transition (SCT). The widely accepted theory on SCT argues that an increase in the evaporation of seawater (or latent heat flux, LHF) is the major driver of the SCT. In this study, we examined this theory using a high-resolution model. To isolate the role of LHF, we did not allow the LHF to adjust to the warming surface and see how the SCT responds. We found that SCT cannot happen if the LHF adjustment is turned off, which confirms the prior theory. However, a key feature of the SCT still persists, namely the decoupling of the stratocumulus from the surface. The decoupling is caused by the weak temperature jump above the cloud, allowing the overlying warm air to sink more effectively into the cloud layer. This process, alone, can induce the decoupling although it cannot sustain the decoupled state without the help of the LHF increase.

1. Introduction

Marine stratocumulus (Sc) has the most extensive areal coverage among all cloud regimes (Hahn and Warren, 2007). This, in combination with their net cooling effect (Hartmann et al., 1992), makes Sc one of the most important players in the Earth's radiative budget (Wood, 2012). An important phenomenon about the Sc is its tendency to transit to cumulus (Cu) clouds as it drifts over warm water (Riehl et al., 1951; Albrecht et al., 1995; Klein et al., 1995; Krueger et al., 1995; Bretherton, 1997; de Roode and Duynkerke, 1997; Zhou et al., 2015; Zheng et al., 2018). Such a cloud transition is well known to predominate over subtropical oceans, where equatorward trade winds generate cold air advection, a necessary condition for the transition to happen. The Sc-to-Cu transition also occurs in the cold section of mid-latitude cyclones (McCoy et al., 2017; kazemirad and Miller, 2020; Zheng et al., 2020) and polar oceans during cold air outbreaks (Abel et al., 2017; Lloyd et al., 2018; Geerts, 2019). Given the substantial impacts of the Sc-to-Cu transition on the regional and global radiative budgets and the difficulty of climate models in simulating it (Teixeira et al., 2011; Bodas-Salcedo et al., 2014; Neggers et al., 2017), it is imperative to continue making progress in understanding its underlying mechanism.

The Sc-to-Cu transition can be divided into two stages (Krueger et al., 1995; Wyant et al., 1997). Consider a radiatively driven well-mixed Sc-topped boundary layer (STBL). In the first stage, as the sea surface temperature (SST) increases, the STBL deepens over time. Accompanied with the deepening is the vertical stratification of STBL into two separate layers, with the upper Sc-containing layer being warmer and drier than the surface mixed layer, a phenomenon called decoupling (Nicholl 1984). After decoupling, Cu often develops on top of the surface mixed layer and detrains water into the Sc deck, forming a Cu-coupled STBL, a consequence of destabilization by cold air advection. In the second stage, as the SST continues to increase, the convection shifts from radiatively driven to surface-flux-driven, manifested as the dominance of cumuliform clouds and eventual dissipation of the stratiform clouds.

The increase in the latent heat flux (LHF) is widely considered the determinant driver of the transition. This view is based on, if not originates from, the theory of deepening-warming decoupling developed by Bretherton and Wyant (1997) (BW97). In the theory, LHF must increase due to the enhanced surface moisture gradient: the surface saturation moisture increases due to the Clausius-Clapeyron relationship, and the near-surface air moisture drops due to the entrainment of dry free-atmospheric air into the boundary layer. With stronger LHF, the buoyancy flux in the cloud layer will strengthen, invigorating cloud-scale turbulence that causes more entrainment warming per unit of cloud-top radiative cooling. This drives both stages of the cloud transition. In the first stage, the enhanced entrainment stabilizes the boundary layer. When the radiative cooling (that varies little relative to entrainment) is not strong enough to mix the entrained warm air throughout the boundary layer, decoupling happens (Lewellen and Lewellen, 1998; Stevens, 2000). In the second stage, the increased LHF invigorates Cu clouds that bump against the inversion, inducing bursts of increased entrainment of dry air into the cloud layer. This eventually dissipates the Sc sheets, leaving only Cu clouds (Wyant et al., 1997). This view of LHF as the driver of Sc-to-Cu transition is supported by a series of high-resolution modeling studies (Wyant et al., 1997; Sandu and Stevens, 2011; Xiao et al., 2011).

Field observations, however, show different results. Jones et al. (2011) found that LHF cannot separate decoupled from well-mixed boundary layers using aircraft data collected over the subtropical southeast Pacifics. Zhou et al. (2015), who used half-year observations collected from

a cargo ship traveling between Los angles, California and Honolulu, Hawaii, found a nearly unchanged LHF along the climatological transact of Sc-to-Cu transition. For this reason, Zhou et al. (2015) argued that the role of LHF in cloud transition is not as determinant as previously thought.

The lack of a clear signal of LHF impact on the transition in observations lends us to ask: how determinant the LHF is for driving the Sc-to-Cu transition? Some clues arise from BW97's own theory. In addition to LHF, other factors can also modify the coupling state of STBL such as the cloud-top radiative cooling, precipitation, and entrainment efficiency. On the time scale characteristic of Sc-to-Cu transition, i.e. multiple days, the radiative cooling and precipitation do not change systematically (or by limited extent), thus their roles are deemed by BW97 as less important. Different is the entrainment efficiency that, in BW97's simulation, systematically increases with the SST, promoting the decoupling in a similar way as the LHF does. The relative importance of the two factors is not thoroughly investigated (BW97 fixes the entrainment efficiency and found decoupling still occurs, however, this cannot demonstrate that LHF is the more dominant factor). One may argue that if the entrainment efficiency is sufficiently large, decoupling may happen regardless of changes in LHF. Indeed, Sandu and Stevens (2011) found that the cloud transition happens faster for an STBL capped by a weaker temperature inversion, a condition favorable for large entrainment efficiency (Nicholls and Turton, 1986). As a result, to what degree the LHF controls the cloud transition should depend on other factors, in particular those controlling the entrainment efficiency (e.g. temperature and moisture jumps across the inversion).

This study aims to elucidate the roles of LHF in driving the Sc-to-Cu transitions using the large-eddy simulations (LESs). Unlike previous LES studies that evaluate the effect of LHF via indirect evidence (e.g. looking at moisture and buoyancy flux profiles), we isolate the role of LHF by turning off the LHF adjustment to the SST increase. Such a mechanism-denial experiment allows for a clearer interpretation of the impact of LHF.

The next section will introduce the model, the experiments, and methods for diagnosing key statistics. The main results are presented in section 3. Sections 4 and 5 are devoted to elucidating the underlying mechanisms of LHF influences on the STBL decoupling (first stage) and Sc dissipation (second stages) during the Sc-to-Cu transition, respectively. In section 4, we will interpret the STBL decoupling using the idea of cloud-layer energy balance developed by BW97. In section 5, dissipations of Sc decks in the control and mechanism-denial experiments will be discussed in the context of the theories of cloud-top evaporative instability (Deardorff, 1980; Randall, 1980) and the cumulus penetrative entrainment (Bretherton, 1997; Wyant et al., 1997). We will quantify the controlling factors of Sc deck lifetime using the liquid water path budget analysis (Van der Dussen et al., 2014). Section 6 and 7 present the discussion and concluding remarks, respectively.

2. Methods

2.1. Model and case description

We use the newest version of System for Atmospheric Modeling (SAM) model, version 6.11.6 (Khairoutdinov and Randall, 2003). SAM is a non-hydrostatic anelastic model. The prognostic thermodynamical scalars are liquid water static energy, total nonprecipitating water

mixing ratio, and total precipitating water mixing ratio. On a fully staggered Arakawa C-type grid, all the prognostic scalars are advected using a three-dimensional positive definite and monotonic scheme developed by Smolarkiewicz and Grabowski (1990). The second-order finite differences in the flux form with kinetic energy conservation are used for momentum. A variable step is adopted for time integration using the third-order Adams–Bashforth scheme. The subgrid-scale turbulence is handled by the 1.5-order subgrid-scale turbulent kinetic energy scheme. A simplified (drizzle only) version of Khairoutdinov and Kogan (2000) microphysics scheme is used for conversion between cloud and rainwater as well as raindrop evaporation and sedimentation. We use the RRTMG as the radiation scheme (Iacono et al., 2008). The surface fluxes are computed from the Monin-Obukhov similarity theory.

This study is based on the simulation of Sc-to-Cu transition during the Atlantic Stratocumulus Transition Experiment (ASTEX) (Albrecht et al., 1995). As shown in Figure 1a, the ASTEX case embarks an evolution of STBL typical of Sc-to-Cu transition: boundary layer deepening, the emergence of sporadic Cu detraining into the Sc deck, and thinning of Sc deck as the Cu develops. During the ASTEX, the SST increases by ~ 4 K over the 40-hour simulation. Here we linearize the SST increase rate, yielding a Tadv = -2.6 K/day (Figure 1c). Such a linearization of SST has the benefit of avoiding unnecessary complications due to a changing surface warming rate. Similarly, we use a diurnally averaged solar zenith angle of 68.72 degrees to remove the influence of the diurnal cycle of solar insolation, because the cloud transition typically has a time scale of multiple days and the diurnal cycle only plays a minor role in the multiple-day transition. Other setups (e.g. initial sounding, mean subsidence, and geostrophic winds) are the same as those used in the ASTEX LES intercomparison project (Van der Dussen et al., 2013). Figure 1b shows the simulated evolution of STBL after the simplifications of surface and radiative forcing. The overall feature of the Sc-to-Cu transition holds well as compared with the original ASTEX simulation (Fig. 1a).

In the control experiment (named “CTRL”), the LHF increases throughout the whole period of the simulation (solid line in Fig. 1c). We run the mechanism-denial experiment by fixing the LHF as the initial value of 67 W m^{-2}, called “FXDLHF”.

The horizontal domain size is 4480^2 m^2 with a horizontal resolution of 35 m. The vertical resolution varies from 15 m at the surface to 5 m in the cloud and the inversion layers. Above ~ 2400 m, the vertical grid size increases by 10% per level until the model top of ~ 4200 m. Increasing the horizontal domain size has a marginal influence on the simulations of weakly precipitating shallow clouds, such as the case in this study (Sandu and Stevens, 2011).

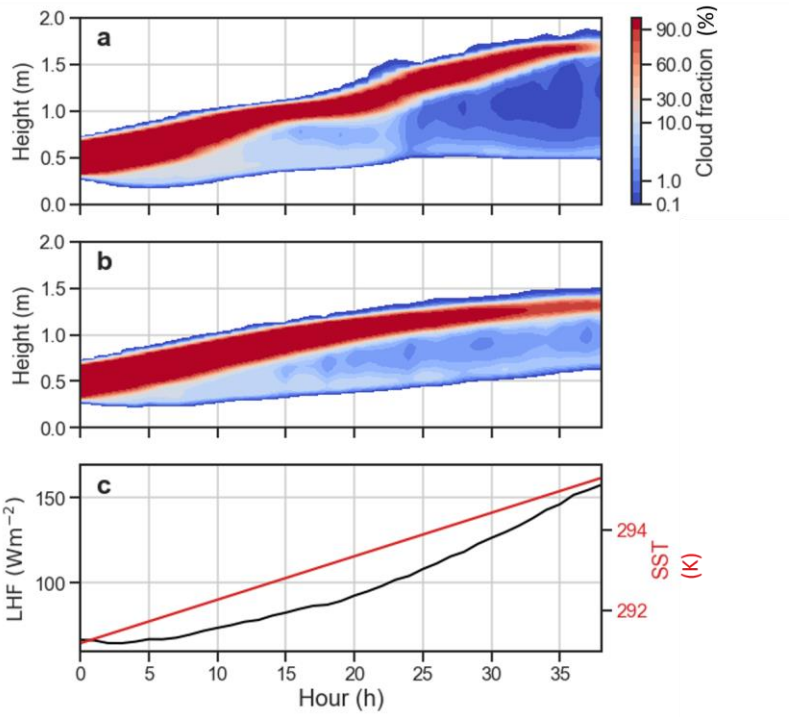

Figure 1: Time-height profiles of SAM-simulated cloud fraction of ASTEX case with original (a) and linearized forcing (b). (c) Temporal evolutions of latent heat fluxes and sea surface temperature (red) for the (b).

2.2. Diagnostic statistics

To measure the degree of boundary layer stratification, we adopt the method of Wyant et al. (1997) to average the liquid water potential temperature (θ_l) over the 75-m layers below the capping inversion and near the surface. Their difference yields the thermal stratification of the STBL, namely $\Delta_{BL}\theta_l$. Similarly, we can diagnose the moisture stratification of $\Delta_{BL}q_t$, in which the q_t is the sum of specific humidity of water vapor (q_v) and liquid water (q_l).

We determine the bottom and top of the capping inversion using the method of Yamaguchi and Randall (2011) that is based on the profile of θ_l variance. This enables quantification of the thermal and moisture jump across the inversion: $\Delta_{inv}\theta_l$ and $\Delta_{inv}q_t$. The cloud-base height of the Sc deck, z_b, is defined as the lowest altitude with cloudiness greater than 50%.

3. Results on the back of the envelope

Figure 2 shows the evolutions of STBL in the CTRL and FXDLHF simulations from which we may infer the influences of LHF as follows.

In the first stage of boundary layer decoupling (the first tens of hours), LHF appears to play no role in the initial decoupling. As shown by the sounding (Fig.2 e and f), both simulations show boundary layers stratifying over the first 15 hours. This trend can be quantified by the evolutions of $\Delta_{BL}\theta_l$ and $\Delta_{BL}q_t$ (Fig. 3) showing an increasing degree of decoupling during t = 0 ~ 15 h for

both runs. From t = 15 h onward, the $\Delta_{BL}\theta_l$ (or the $\Delta_{BL}q_t$) starts to diverge between the two runs. In the FXDLHF, the boundary layer recouples, as seen from the decreased stratification (Fig. 3) and the reduced distance between the base of the Sc deck and LCL (Fig. 2c). The results suggest that fixing the LHF does not prevent the boundary layer from decoupling, but the decoupled state cannot sustain.

In the second stage of Sc dissipation, fixing the LHF eventually results in a cloud-free boundary layer without any Cu clouds left. Sc decks dissipate in both simulations but in different ways. In the CTRL, the Sc deck breaks up as the cumulus clouds shooting into the Sc deck (Fig. 2a), a regime characteristic of the typical Sc-to-Cu transition. In the FXDLHF, however, the Sc sheet dissipates in a well-mixed STBL in which the drying of the boundary layer (Fig. 2f) elevates the LCL. The LCL gradually approaches the boundary layer top, thinning the Sc deck over time (Fig. 2c). This eventually leads to a clear boundary layer. Such a difference of the Sc dissipation between the two runs can also be seen from the dynamic fields (e.g. vertical velocity variance shown in Fig. 2b and d). In the CTRL, the vertical velocity variance has two separate peaks during the break-up, one below the inversion and one in the sub-cloud layer, which is a manifestation of the Cu-fed Sc regime. In the FXDLHF, the vertical velocity variance profile tends toward a single peak from t = 50 h onward when the dissipation kicks off, a manifestation of a well-mixed STBL. Interestingly, the Sc deck sustains longer in FXDLHF than the CTRL run (Fig. 3c).

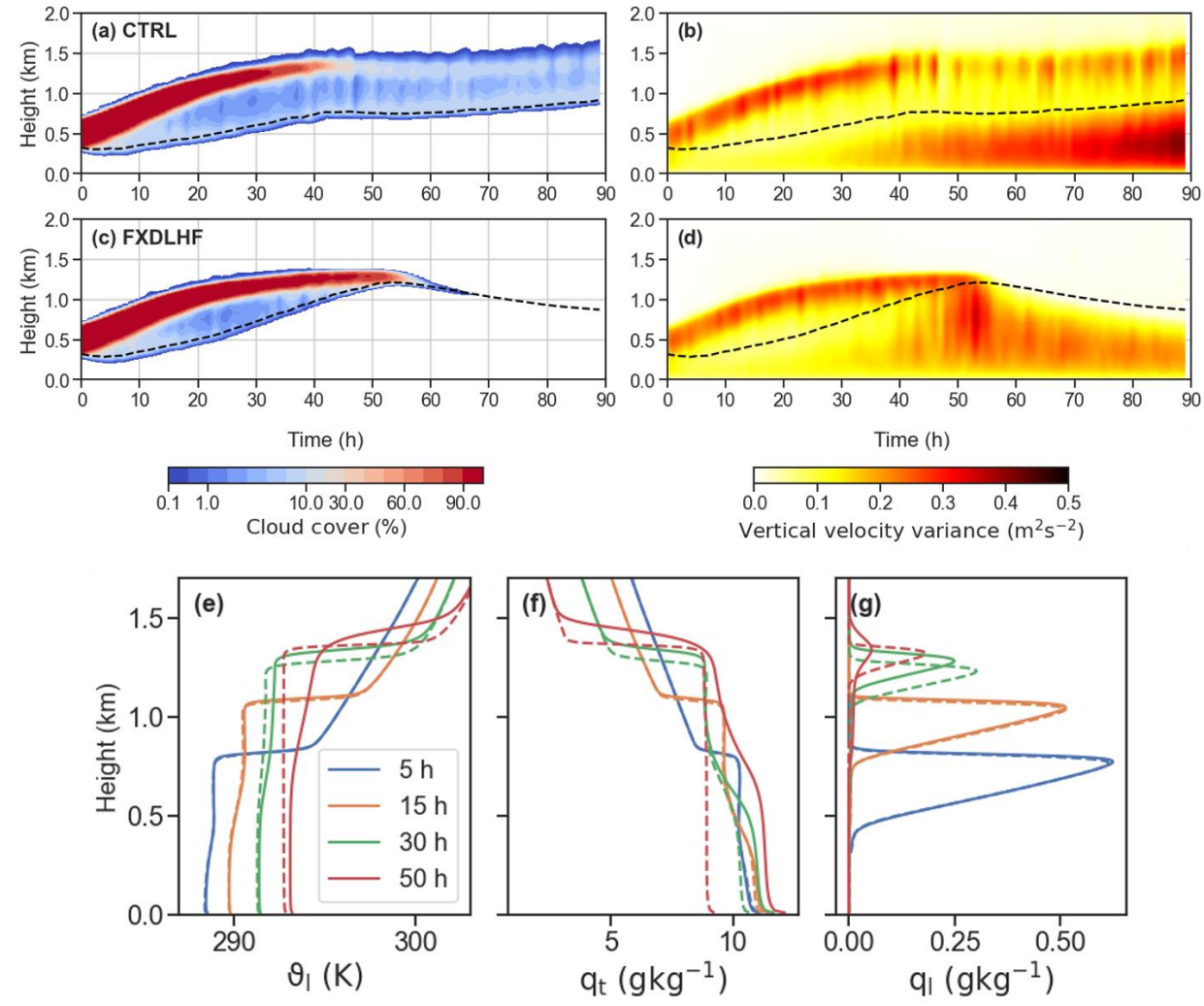

Figure 2: Evolutions of STBLs in CTRL and FXDLHF runs. (a)~(d) shows the time-height plots of cloud fraction and vertical velocity variance for the CTRL (a and b) and FIXDLHF (c and d). The dashed line marks the lifting condensation level. (e)~(g) shows the vertical profiles of θ_l, q_t, and q_l for CTRL (solid) and FXDLHF (dashed) at different times of the simulations.

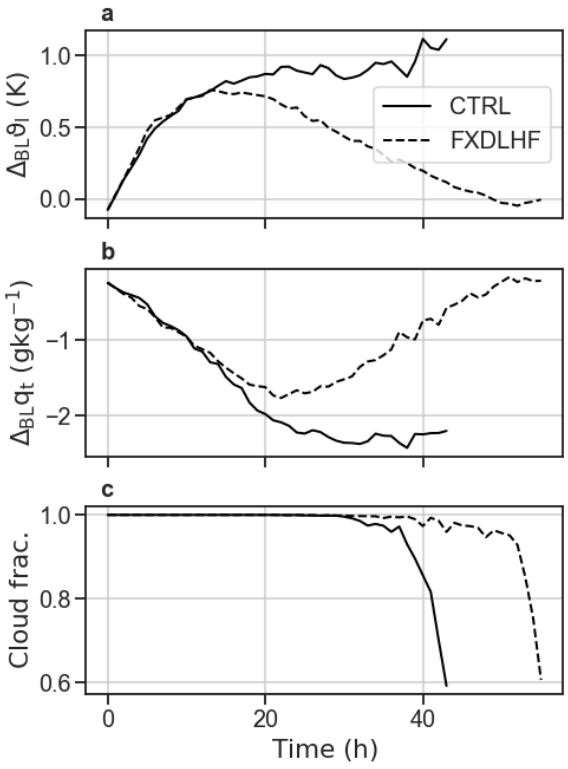

Figure 3: Temporal evolutions of the boundary layer thermal (a) and moisture (b) stratifications and cloud fraction (c).

In a summary, decoupling happens in both runs, but the decoupled state cannot sustain in the FXDLHF in which the decoupled boundary layer eventually recouples. In the FXDLHF, the lack of moisture supply from the surface dries the boundary layer over time, which eventually dissipates the Sc deck, leading to a clear boundary layer. Therefore, the transition to Cu regime does not happen without an increase in LHF. Despite the lack of moisture supply in FXDLHF, Sc deck sustains longer by ~ 10 hours than that in CTRL.

A series of questions arise: Why does decoupling still happen even if the LHF is not allowed to increase? Why does the boundary layer recouple after initial decoupling in the FXDLHF? Can the FXDLHF results be explained by the theoretical framework of BW97? Why does the Sc sustain longer when the surface moisture supply is weaker? How to explain the Sc dissipations in both runs with existing theories such as the cloud-top entrainment instability (Randall 1980; Deardoff 1980) and "cumulus penetrative entrainment" theory (Wyant et al., 1997)?

To answer these questions, we will delve into the underlying mechanisms of the STBL decoupling and cloud dissipation in sections 4 and 5, respectively.

4. First stage: STBL decoupling

4.1. A theoretical inquiry

We use the cloud layer energy balance to guide our investigation, inspired by BW97. We begin by considering a variable that measures the buoyancy for cloudy air, namely the virtual liquid water potential temperature:

$$\theta_{vl} = \theta_l + (0.61\theta_{ref})q_t, \qquad (1)$$

in which the θ_{ref} is a reference potential temperature, taken as a fixed value (290 K) representative for the cloud layer. The θ_{vl} is physically similar to the density potential temperature in Emanuel (1994) and Stevens (2007) and the liquid-water virtual static energy in BW97.

There are two benefits of using θ_{vl}. First, it is a linear combination of two adiabatically conserved variables (i.e. θ_l and q_t), which renders its analytical treatment easier. Second, in unsaturated flow, the $\theta_{vl} = \theta_v$. This bridges the θ_{vl} budget in the cloud layer to the sub-cloud buoyancy flux through the $\overline{w'\theta_{vl}'} = \overline{w'\theta_v'}$ at $z = z_b$. As will be elaborated later, this association is crucially important for understanding the STBL decoupling.

To derive a budget equation for θ_{vl} in the cloud layer, we start with the budget equations for θ_l and q_t:

$$h\frac{\partial \theta_l}{\partial t} = w_e\Delta_{inv}\theta_l - \frac{1}{\Pi}\left(\Delta F_{rad} - \frac{L_v}{c_p}\Delta P\right) + \overline{w'\theta_l'}(z_b) \qquad (2a)$$

$$h\frac{\partial q_t}{\partial t} = w_e\Delta_{inv}q_t - \Delta P + \overline{w'q_t'}(z_b), \qquad (2b)$$

in which w_e is the entrainment rate across the inversion (m s^{-1}), F_{rad} is the net radiative flux (K m s^{-1}), Π is the Exner function, P is the precipitation rate (m s^{-1}), and $\overline{w'\theta_v'}(z_b)$ and $\overline{w'q_t'}(z_b)$ are eddy fluxes of θ_l and q_t at cloud base, respectively. The Δ_{inv} and Δ denote the differences across the inversion layer and cloud layer, respectively. Combining (2a) and $0.61\theta_{ref}$×(2b) yields:

$$\underbrace{h\frac{\partial \theta_{vl}}{\partial t}}_{Stor} = \underbrace{w_e\Delta_{inv}\theta_{vl}}_{Ent} \underbrace{- \frac{\Delta F_{rad}}{\Pi}}_{Rad} + \underbrace{\left(\frac{L_v}{c_p\Pi} - \mu\right)\Delta P}_{Prec} + \underbrace{\overline{w'\theta_{vl}'}(z_b)}_{Base}, \qquad (3)$$

in which the μ=$0.61\theta_{ref}$. The budget terms from the left to the right are storage term (*Stor*), entrainment warming (*Ent*), diabatic cooling by radiation (*Rad*), diabatic heating by precipitation (*Prec*), and θ_{vl} flux through the cloud base (*Base*). *Rad* + *Prec* yields the diabatic cooling term, denoted as *Diab*.

The budget formula can help us understand the STBL decoupling. A key signature of STBL decoupling is the emergence of negative buoyancy fluxes below the cloud base (Bretherton, 1997; Stevens, 2000). The more negative the downward buoyancy flux is, the more likely the STBL is decoupled. At the cloud base, the buoyancy flux $\overline{w'\theta_v'} = \overline{w'\theta_{vl}'}$ that is the *Base* term in Eq. (3). Thereby, STBL decoupling can be understood as the *Base* term smaller than a negative critical value. Assuming the *Stor* term maintains considerably smaller than the forcing terms, the following processes, via favoring a decrease in *Base*, promote the decoupling:

- An increase in the entrainment.
- A decrease in the cloud-top radiative cooling.
- An increase in the precipitation.

The three decoupling-promoting processes are consistent with our previous knowledge (Nicholls, 1984; Nicholls and Leighton, 1986; Bretherton, 1997; Wood, 2012). This framework can help us conceptualize how LHF is associated with the STBL decoupling. An increase in LHF will strengthen the buoyancy in the cloud layer through latent heating, increasing the $\overline{w'\theta_v'}$ averaged over the boundary layer, denoted as $\langle\overline{w'\theta_v'}\rangle$. The increased $\langle\overline{w'\theta_v'}\rangle$ will increase the *Ent* according to the entrainment closure of Turton and Nicholls (1987):

$$w_e\Delta_{inv}\theta_v = A\langle\overline{w'\theta_v'}\rangle, \quad (4)$$

in which the *A* is a non-dimensional parameter dictating the entrainment efficiency, which measures the entrainment rate for a given buoyancy inversion and turbulence level. Therefore, an increase in LHF promotes decoupling. This is the key idea of BW97's deepening-warming theory.

The above discussion offers several important insights into the relationship between the LHF and decoupling. First, it is the absolute value of LHF, not its temporal evolution, that directly determines the STBL decoupling. Imagine an STBL starting with an LHF large enough to cause excessive entrainment warming than the diabatic cooling, the STBL will decouple even if the LHF remains unchanged (or even decreases over time). In that regard, observations of unchanged LHF along the Sc-to-Cu transitions cannot disapprove of the deepening-warming theory (e.g. Zhou et al., 2015). Second, in addition to the LHF, the entrainment efficiency, *A*, is equally important in determining the decoupling. According to Eq. (4), an increase in *A* can yield the same results as the enhanced LHF does. Past works suggest that the *A* should increase with the cloud-top evaporative cooling (Nicholls and Turton, 1986) and radiative cooling, with both dependent upon the properties of the cloud layer (e.g. liquid water content) and inversion layer (e.g. thermodynamic properties of the overlying air). There is also evidence suggesting that the regime of boundary layer turbulence (e.g. cumulus-like versus stratocumulus-like) can modify the *A* (Wyant et al., 1997).

4.2.Mixed-layer model simulation

To elucidate the role of LHF, we run the mixed-layer model (MLM) (Lilly, 1968; Bretherton and Wyant, 1997; Bretherton et al., 2010) to examine how the budget terms in Eq. 3 evolve during the transition. An important merit of MLM is its analytic tractability, which helps us understand the "coarse-grain" behavior of the system.

The MLM we use is the same as that used in BW97. The model has three prognostic equations for the boundary layer depth, moist static energy, and q_t, which describes the budgets of mass, enthalpy, and moisture, respectively. In the MLM, the *A* is parameterized as (Nicholls and Turton, 1986):

$$A = 0.2[1 + 60(1 - \frac{\Delta_m}{\Delta_{inv}s_v})], \quad (5)$$

in which $\Delta_{inv}s_v$ is the difference in virtual static energy (s_v) across the inversion and the Δ_m is twice the average of the difference between the s_v of entrained air across the inversion and the s_v of the saturated air at the cloud top. As elaborated in Nicholls and Turton (1986), the *A* is a measure of the strength of evaporative cooling. Physically speaking, a weaker buoyancy inversion, drier free-atmosphere, and juicier clouds favor the evaporation of cloud water, although the quantitative detail of their combined control is more complex. Note that Eq. (5) is an idealized approximation of the *A* and we use it for illustrative purposes only. Strictly speaking, it does not explicitly include some factors such as the radiative cooling (Stevens, 2002), cloud droplet sedimentation (Bretherton et al., 2007), and other less known *A*-controlling factors such as the turbulence regime (Wyant et al., 1997).

The MLM diagnoses the decoupling based on the buoyancy integral ratio (*BIR*) defined as $-\frac{\int_0^{z_i}\overline{w'\theta_v'}\mathcal{H}(-\overline{w'\theta_v'})dz}{\int_0^{z_i}\overline{w'\theta_v'}\mathcal{H}(\overline{w'\theta_v'})dz}$, in which the $\mathcal{H}$ is the Heaviside function. The physical meaning of *BIR* is the vertical integral of the negative buoyancy flux divided by the vertical integral of the positive buoyancy flux. Following the BW97, we use a *BIR* threshold of 0.15, above which the STBL is considered decoupled and the MLM ceases to be valid.

We specify the radiative cooling as 60 Wm^{-2} throughout the simulations. Time variations of the radiative cooling, either in diurnal or multiple-day time scales, have marginal influences on the systematic cloud transitions (Bretherton, 1997; Bretherton and Wyant, 1997). Fixing it has the benefit of simplifying the analysis, allowing us to focus on the role of LHF.

We first run a control case in an environment typical of the subtropical eastern Pacific. The case setup is the same as BW97 (see their Table 1 for simulation parameters). To summarize briefly, the initial SST is 285 K that increases by 1.5 K/day. The initial capping inversions of temperature and moisture are 13.2 K and -4.2 g kg^{-1}, respectively. The large-scale divergence, horizontal wind, and free tropospheric moisture are held constant throughout the simulation. Fig 4a shows the evolutions of the boundary layer of the control case. The STBL deepens over time, accompanied by increasingly negative buoyancy flux below the cloud base, which eventually causes decoupling.

Such a decoupling process can be understood from the perspective of the cloud-layer energy budget (Fig. 4d). The *Ent* increases throughout the simulation, whereas the *Diab* changes very little. Such excessive warming has two consequences. First, the cloud layer heats up (i.e. *Stor* increases). Second, to balance the excessive warming, the buoyancy flux near the cloud base must shift from upward to downward (i.e. *Base* decreases), eventually causing decoupling.

Increases in LHF and *A* jointly contributes to the decoupling. The role of LHF is clearly seen on the first day when the LHF increases rapidly, raising the turbulence level (Fig. 4b). The stronger turbulence is responsible for the initial increase in the *Ent*, an expected consequence of Turton and Nicholl (1986)'s entrainment closure. From the first day onward, as the STBL deepens and erodes into the dry free atmosphere, the *A* increases (Fig. 4c), further strengthening the *Ent*. Such strengthened entrainment tends to suppress the boundary layer turbulence even though the LHF keeps increasing. Overall, increases in LHF and *A* jointly enhance the *Ent* that drives the decoupling.

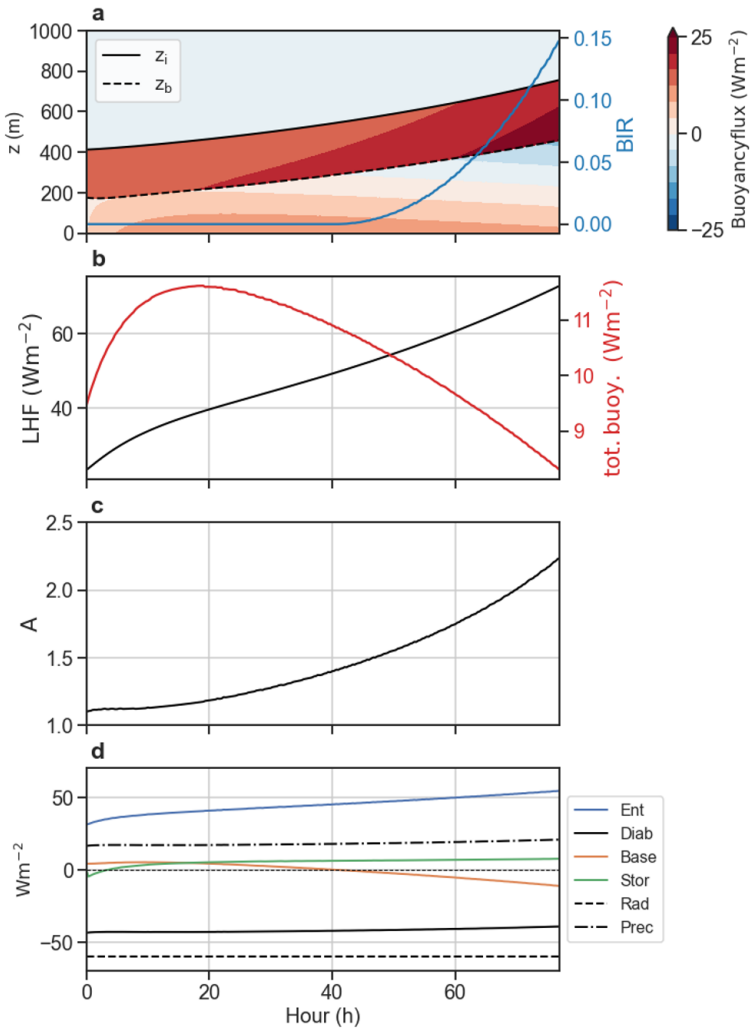

Figure 4: MLM simulation of the control case. (a) shows a time-height plot of buoyancy flux and time evolutions of cloud boundaries and *BIR*. Temporal evolutions of LHF and STBL-averaged buoyancy flux (b), entrainment efficiency (c), and cloud-layer energy budgets (d).

To examine the individual roles of LHF and *A*, we run two simulations by fixing the *A* and LHF as their respective initial values (Figure 5), noted as "FXDA" and "FXDLHF", respectively. In FXDA, the boundary layer still decouples but at a much slower rate than the control case. Without the adjustment in *A*, an increase in LHF strengthens the boundary layer turbulence and deepens the cloud depth via more latent heating and moisture supply, respectively. These two effects cause enhanced *Ent* and *Prec*, both promoting decoupling. However, the increasing rate of *Ent* is considerably slower than the control case due to the fixed *A* (Fig. 5). This, again, supports the importance of *A* feedback in decoupling.

In the FXDLHF run, the STBL remains coupled throughout the simulation. Without the increase in LHF, *Ent* remains noticeably smaller than the *Diab*. To balance the excessive cooling, the system must maintain a positive *Base*, which sustains the well-mixed STBL. More importantly,

the relatively weak entrainment prevents the boundary layer from deepening so that the property of the capping inversion varies little, leading to a little varied *A*. Actually, the *A* decreases slightly due to the shallowing of the boundary layer. This helps maintain the coupling state.

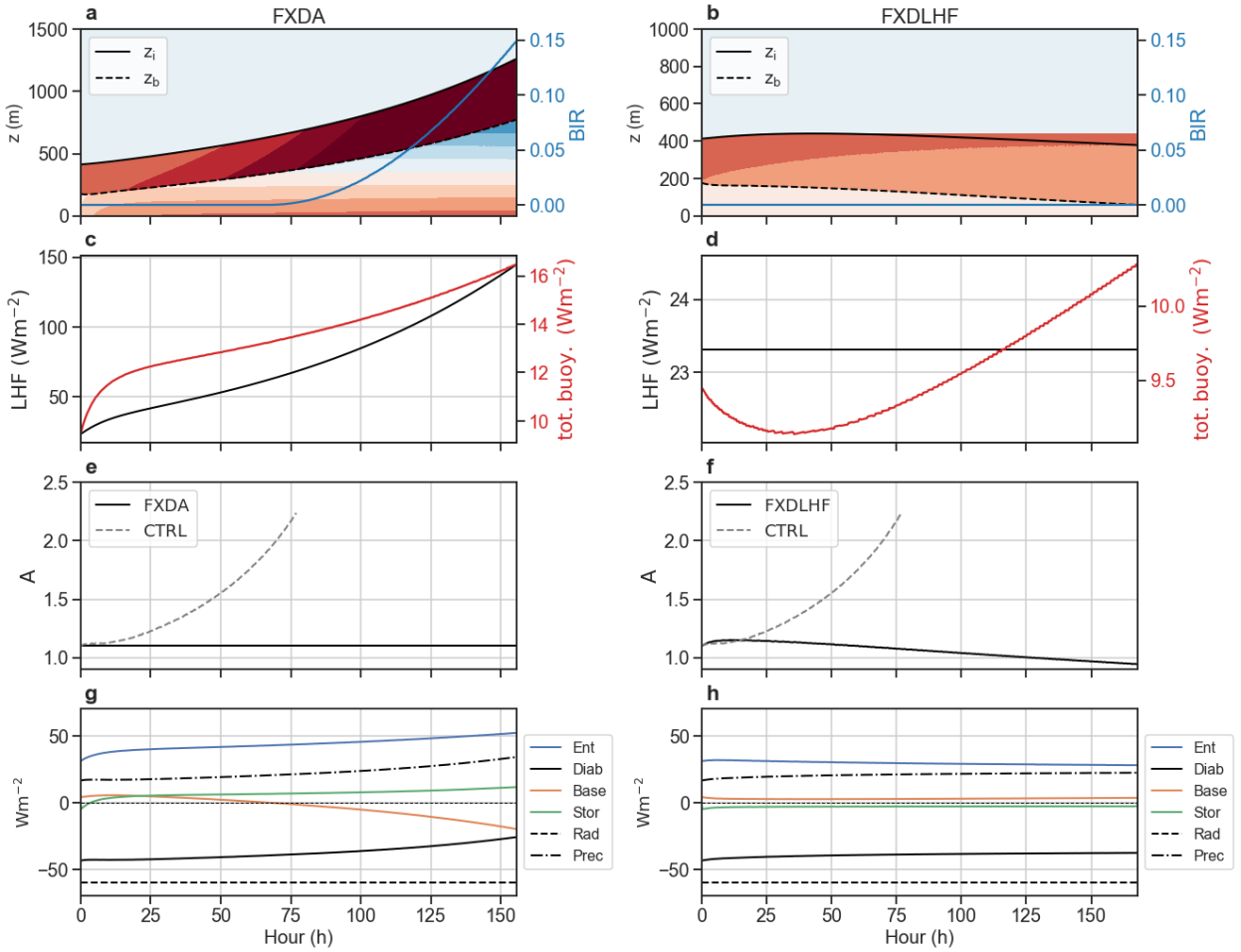

Figure 5: Same as Figure 4 but for FXDA (left) and FXDLHF (right) cases. The time variation of *A* in the control case is plotted in (e) and (f) as a reference.

In addition to confirming BW97's idea that increasing the LHF alone is enough to drive decoupling, the above analysis stresses the significant role of the feedback associated with *A*. Compared with the control case, the *A* in both simulations are considerably smaller, leading to either much slower decoupling (FXDA) or no decoupling at all (FXDLHF), pending on the LHF. Such an important role of *A* may help us explain why the boundary layer decouples in the first 15 hours of the LES FXDLHF experiment (Fig. 3). Unlike the MLM case that is capped by a strong inversion with a temperature jump of 13.2 K, the LES case (i.e. ASTEX) has a $\Delta_{inv}\theta_l$ of only 5.5 K. Everything else being equal, a weaker inversion typically corresponds to a larger *A* (Nicholls and Leighton, 1986), promoting the decoupling. To test this hypothesis of *A*-induced decoupling, we repeat the MLM FXDLHF experiment, but initialize the case with a weaker temperature inversion (half as much). As shown in Figure 6, the STBL decouples after ~20 hours. Although

the increase in *Prec* term contributes considerably to the eventual decoupling, the weak inversion maintains a large *A*, which sustains a large *Ent* throughout the simulation, allowing the decoupling to happen. This result is consistent with the finding from Sandu and Stevens (2011) that the Sc-to-Cu transition happens faster if the capping inversion is weaker.

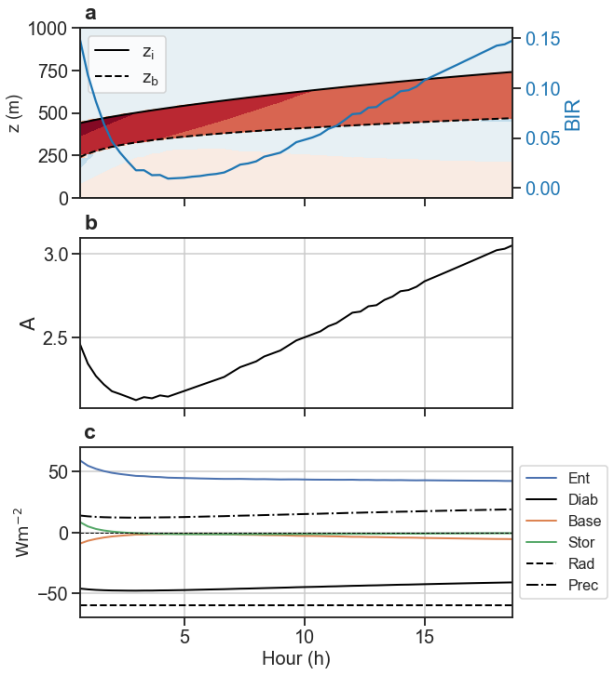

Figure 6: Same as Figure 4 but with fixed LHF and halved initial temperature jump across the capping inversion.

In a summary, we learn two lessons from the MLM simulations. First, for a given diabatic cooling, decoupling is jointly controlled by the surface forcing (via the LHF) and the overlying atmospheric stability and humidity (via the *A*). Second, the relative magnitude of *Ent* and *Diab* is a diagnostic variable useful for understanding the decoupling. This can be well illustrated in Figure 7 showing the evolutions of *Ent* + *Diab* and *BIR* for the four MLM simulations: CTRL, CTRL FXDA, CTRL FXDLHF, and WEAK INV FXDLHF. STBLs with larger *Ent* + *Diab* are more likely to decouple and decouples at faster rates. This makes the *Ent* + *Diab* a useful parameter to interpret LES results. A long-lasting challenge of interpreting LES-simulated decoupling is that the geometry of the buoyancy flux profile is more complicated in LES than in MLM. As argued by Lewellen and Lewellen (1998), an increase in entrainment tends to weaken the STBL-integrated buoyancy not only by increasing negative buoyancy fluxes in the sub-cloud layer but also by modifying the entire buoyancy geometry in a way that remains poorly understood. For example, if the radiative cooling concentrates at a thinner-than-usual layer, the entrained warm air may be cooled to the extent that negative buoyancy flux does not occur at any level even though the energetic cost of the entrainment still exists, manifested by lessened positive buoyancy flux.

Moreover, under the condition of cold advection, the occurrence of cumulus-coupled STBL further complicates the geometry of the buoyancy flux profile (Bretherton and Blossey, 2014). These issues could be circumvented by using *Ent* + *Diab* as a physically solid diagnostic to interpret decoupling.

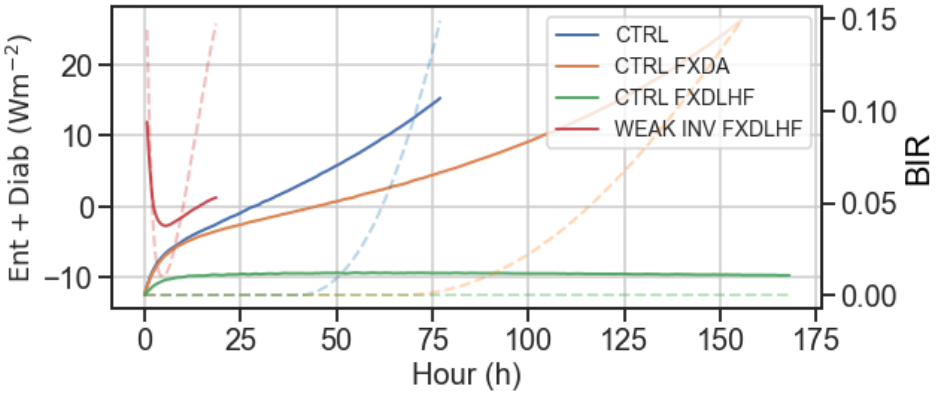

Figure 7: The capability of *Ent* + *Diab* in dictating decoupling. Temporal evolutions of *Ent* + *Diab* (solid) and *BIR* (dashed).

4.3.LES

After the theoretical and MLM inquiries, we return to interpreting the LES simulations. In particular, we will utilize the *Ent* + *Diab* to interpret the time evolutions of decoupling. The *Diab* term can be easily diagnosed from the profiles of radiative and precipitation fluxes simulated by the LES. The entrainment rate, w_e, is diagnosed from the mass budget equation: $w_e = dz_i/dt - w_{sub}$, in which the z_i is the inversion-layer height and the w_{sub} is the subsidence rate evaluated at z_i. Figure 8a shows the evolutions of *Ent* + *Diab* for the LES CTRL (solid red) and FXDLHF runs (dashed red). The *Ent* + *Diab* is markedly positive in the beginning 15 hours for both simulations. Such sizable excessive heating explains the STBL decoupling (Fig. 8e and f). Although the radiative cooling increases by ~ 10 W m^{-2} during the period of the first 15 h (Fig. 8b), the entrainment heating increases (Fig. 8c) by a larger extent (~ 25 W m^{-2}), so that the *Ent* + *Rad* overall increases. The *Prec* initially increases but decreases after t = 6 h, which is responsible for the inverted-U shape of the *Ent* + *Diab*, but does not alter the overall increasing trend of the *Ent* + *Diab* during t = 0 ~ 15 h. From t = 15 h onward, the two curves of *Ent* + *Diab* diverges. In FXDLHF, the decreasing trend of *Ent* + *Diab* well explains the recoupling of the boundary layer after t = 15 h (Fig. 8e). In CTRL, the *Ent* + *Diab* remains large, explaining the sustained decoupling.

Such a diverge of *Ent* + *Diab* between the two experiments reflects the role of LHF. In the FXDLHF run, without an increase in LHF, the large entrainment rate is difficult to sustain (Fig. 8f). The reasons are threefold: (1) the temperature jump across inversion increases (Fig. 8g); (2)

precipitation decreases (Fig. 8d) and (3) radiative cooling strengthens (Fig. 8b), all promoting re-coupling. In the CTRL, the increasing LHF generates sufficient in-cloud buoyancy to sustain the w_e (Fig. 8f) so that the *Ent* remains large enough to overcome the diabatic cooling, thereby maintaining the decoupled state (Fig. 8a). Such large entrainment also dries the cloud liquid water more effectively, eventually reducing the *Rad* (Fig. 8b), which constitutes positive feedback that breaks up the stratocumulus decks.

In a summary, the evolution of the STBL coupling state can be well explained by the *Ent* + *Diab*. By fixing LHF, decoupling can still occur because the initial *Ent* + *Diab* is large enough to promote the decoupling. Such decoupling can only sustain for 15 hours, after which the boundary layer recouples primarily due to the LHF not sufficiently large to sustain the entrainment.

What causes such a large *Ent* + *Diab* at the beginning? As discussed in the MLM simulations, a large *Ent* can be attributed to a large *A* that is sensitive to the mixing properties between the Sc deck and the overlying air of the capping inversion. The ASTEX case has a $\Delta_{inv}\theta_l$ of only 5.5 K, which is smaller than typical extensive Sc decks over the eastern subtropics (Wood and Bretherton, 2006). This favors more efficient entrainment and, thus, large *Ent* + *Diab*. To test the hypothesis, we repeat the two LES experiments by doubling the $\Delta_{inv}\theta_l$ of the initial sounding. The two new experiments are named "STRGINV" and "STRGINV FXDLHF", respectively. To infer the *A* from the LES data, we use the Eq. 4. We replace the vertically averaged buoyancy flux with the turbulent dissipation averaged over the 200 m below the capping inversion because the latter is suggested to better represent the turbulence effect on entrainment (Bretherton and Blossey, 2014).

The two new runs with stronger inversion are marked by the blue lines in Figure 8. Indeed, the *A* is substantially smaller when the inversion strength doubles (Fig. 8h). The smaller *A* leads to smaller *Ent* (Fig. 8c) and thus smaller *Ent* + *Diab* (Fig. 8a), resulting in more coupled STBLs (Fig. 8e and f). This confirms our hypothesis. Comparing the STRGINV and STRGINV FXDLHF leads to similar conclusions on the role of LHF in decoupling that has already been discussed.

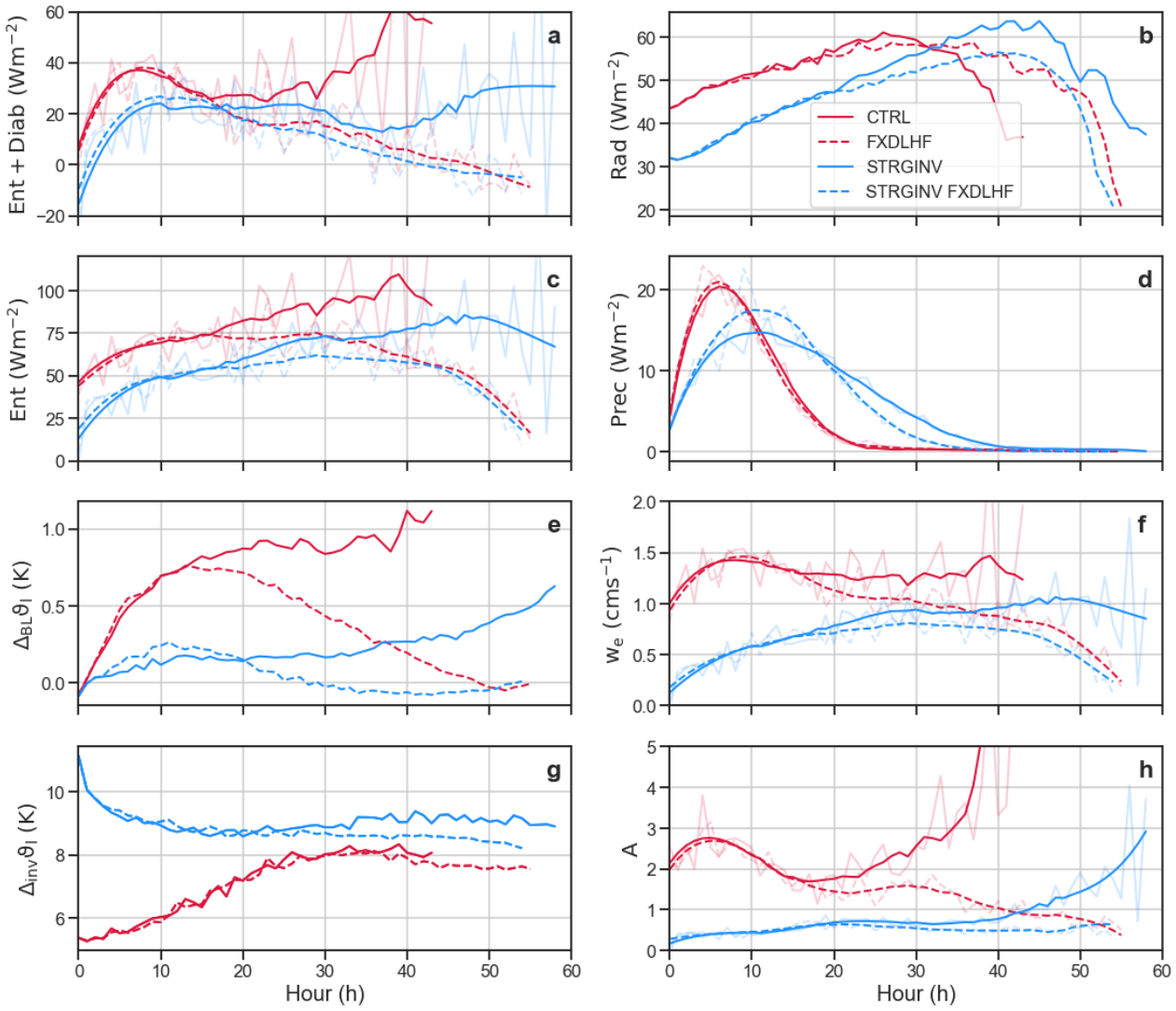

Figure 8: Temporal evolutions of key LES diagnostics for the four LES experiments. Variables diagnosed from w_e are smoothed to more clearly reflect the trend (intermittent cumulus convection causes large variances in these quantities). The unsmoothed values are marked by the semi-transparent lines.

5. Second stage: dissipation of stratocumulus deck

Fixing the LHF delays the break-up of the stratocumulus sheet by ~ 10 hours (Fig. 3c). This section aims to figure out what causes the late dissipation.

There are two potential mechanisms for the dissipation. The first is the theory of cloud-top entrainment instability (CTEI) (Lilly, 1968; Deardorff, 1980; Randall, 1980). This mechanism is based on the idea that the warm and dry air entrained across the inversion can mix with the saturated air. The evaporative cooling of the mixture can, in certain conditions, lead to negatively

buoyant downdrafts, which enhances the entrainment by generating the TKE, forming a positive effect. Such a runaway effect dissipates the clouds. This mechanism is expressed in terms of a parameter $\kappa = 1 + \frac{c_p}{L_v}\frac{\Delta\theta_l}{\Delta q_t}$. The runaway effect can occur if the κ is greater a critical value although the exact threshold remains controversial (Kuo and Schubert, 1988; Siems et al., 1990; Siems and Bretherton, 1992; Stevens et al., 2003; Yamaguchi and Randall, 2008; Lock, 2009; Van der Dussen et al., 2014).

The second mechanism is proposed by Wyant et al. (1997) who argue that the breakup of Sc deck is caused by the Cu penetrative entrainment (CuPE). They found that in the Cu-fed Sc regime the Cu convection can both desiccate and moisten the Sc by promoting entrainment drying and by enhancing upward fluxes of moisture, respectively. The ratio between the two, defined as the "cumulus entrainment efficiency", gradually increases as the STBL deepens, which acts to dissipate the Sc deck.

The two mechanisms focus on different aspects of Sc dissipation. The CTEI stresses the significance of jumps of moisture and temperature above the Sc deck whereas the CuPE centers on the preexisting turbulence in the boundary layer. More often than not, these two processes couple with each other so that separating them is practically challenging.

Serendipitously, our LES simulations (i.e. CTRL versus FXDLHF) are well suitable for comparing the two. The reason is that inversion properties are similar between the two experiments whereas the boundary layer regimes during dissipations are dramatically different: Cu-coupled STBL in CTRL versus well-mixed STBL in FXDLHF. This constitutes a control experiment as the mechanism of CuPE operates in CTRL, but not in FXDLHF that is absent of Cu convection. The difference can be clearly seen in Figure 9 showing the profiles of vertical velocity skewness during the breakup stages. We know that the sign of vertical velocity skewness reflects the driver of buoyancy (Moeng and Rotunno, 1990), with positive and negative values suggesting bottom-heating-driven and top-cooling-driven, respectively. In the CTRL, the vertical velocity variance is typical of a Cu-coupled STBL in which the cloud-top radiative cooling and surface heating jointly drive the convection, leading to a mixture of positive and negative skewness (Fig. 9a). In contrast, convection in FXDLHF is primarily driven by cooling from above, as manifested by negatively skewed vertical velocities throughout most of the boundary layer except close to the inversion.

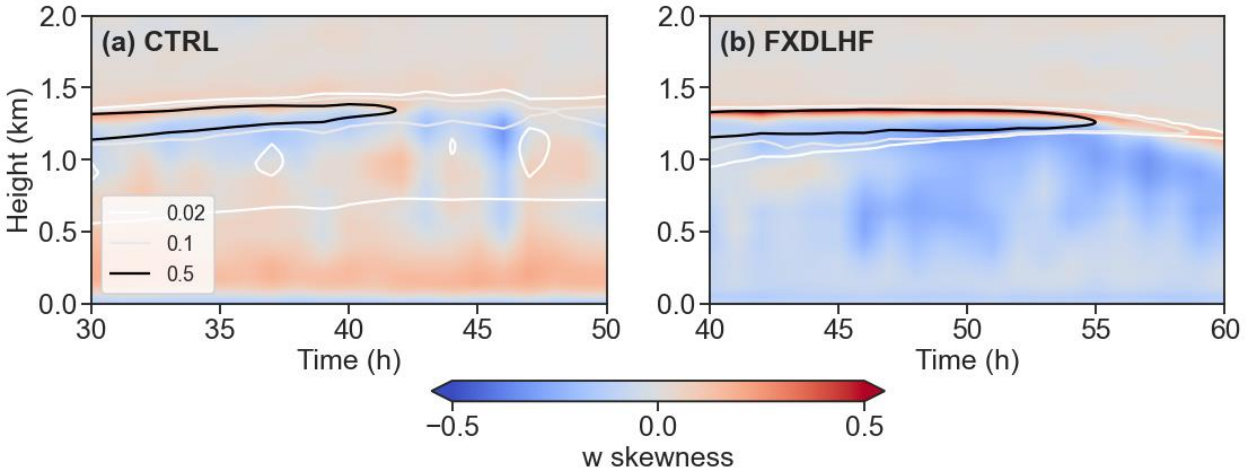

Figure 9: Time-height plot of the vertical velocity skewness during the breakup stage for CTRL (30 ~ 50 h) and FXDLHF (40 ~ 60 h). The lines mark the cloud cover (unitless).

Figure 10 shows the cloud fraction versus κ. Both simulations show that cloud fraction decreases with κ, generally consistent with the CTEI theory, but their relationships differ in two respects. First, the change of cloud fraction with κ is more rapid in FXDLHF than in CTRL. The rapid dissipation eventually leads to a clear boundary layer, which behaves like a quick runaway process. This is consistent with the CTEI theory that predicts an unstable process driven by positive feedback. In contrast, the cloud fraction in CTRL gradually evolves from the Sc regime with full coverage to the Cu regime with a cloud cover of ~ 20%, consistent with the CuPE.

Second, Sc breaks up at a smaller κ in the CTRL than in FXDLHF. This appears to be a manifestation of the additional drying effect of the CuPE mechanism that only operates in CTRL run (CTEI should operate in both). This enhanced drying by CuPE is supported by the larger q_t flux at the cloud base in CTRL. According to Van der Dussen et al. (2014), CTEI predicts that larger cloud-base moisture flux enables the Sc deck to sustain at a larger κ because of the more moisture supply compensating for the CTEI-induced desiccation. This argument from the CTEI-based reasoning is not supported by our simulations: Sc breaks up at a smaller κ when the cloud-base q_t flux is large. Such a result is more consistent with the CuPE theory predicting that dissipation is accompanied by stronger q_t flux at Sc base.

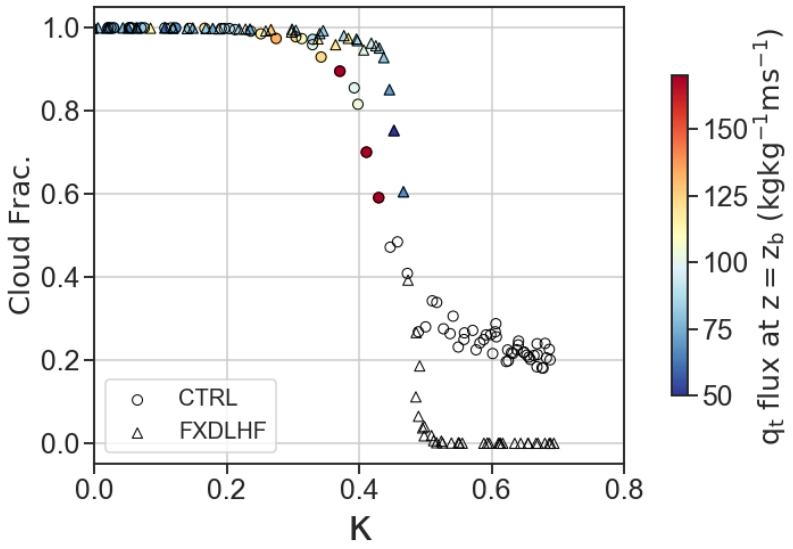

Figure 10: Cloud fraction versus κ for CTRL and FXDLHF runs. Symbols are color-coded by the q_t flux at Sc cloud base (only those with cloud fraction greater than 0.5).

The above analysis confirms the role of Cu convection in breaking up the Sc deck. By not allowing the LHF to increase, Cu convection cannot develop so that the mechanism of CuPE is absent, leaving only the CETI mechanism to operate. This can postpone the dissipation of Sc deck, but, once the CETI initiates, a runaway effect dominates, shifting a well-mixed STBL to a clear boundary layer.

To further confirm the CuPE-induced drying, we use the budget analysis of LWP (Van den Dussen et al., 2013):

$$\frac{\partial LWP}{\partial t} = Ent_{LWP} + Base_{LWP} + Rad_{LWP} + Prec_{LWP} + Subs_{LWP}, \qquad (6)$$

in which

$$Ent_{LWP} = \rho w_e(\eta \Delta q_t - \Pi\gamma\eta\Delta\theta_l - h\Gamma_{q_t}), \qquad (6a)$$

$$Base_{LWP} = \rho\eta(\overline{w'q_t'}(z = z_b) + \Pi\gamma\overline{w'q_t'}(z = z_b)), \qquad (6b)$$

$$Rad_{LWP} = \rho\eta\gamma\Delta F_{rad}, \qquad (6c)$$

$$Prec_{LWP} = -\rho\Delta P, \qquad (6d)$$

$$Subs_{LWP} = -\rho h\Gamma_{q_t} w_{sub}. \qquad (6e)$$

The five forcing terms on the right-hand side of the equation represent the entrainment, turbulent fluxes at cloud base, radiation, precipitation, and subsidence, respectively. We use the subscript "LWP" to distinguish them from the terms in the budget equation of θ_{vl}. Figure 11 shows the temporal evolutions of all the forcing terms in CTRL (solid) and FXDLHF (dashed) runs. In the CTRL run, the stronger LHF leads to more moisture supply to the cloud layer, as shown by the

$Base_{LWP}$ term. However, the larger LHF also strengthens the entrainment drying (Ent_{LWP}), disiccating the clouds. The entrainment drying starts to outweigh the moistening effect after t = 20 h as the Cu convection develops. Throughout the simulations, the combined effects of the changes in $Base_{LWP}$ and Ent_{LWP} due to the larger LHF is to dry the clouds, as shown by the more negative Ent_{LWP} + $Base_{LWP}$ for the CTRL run (brown lines). This finding supports the role of LHF in invigorating the Cu convection, promoting the breakup of the Sc deck.

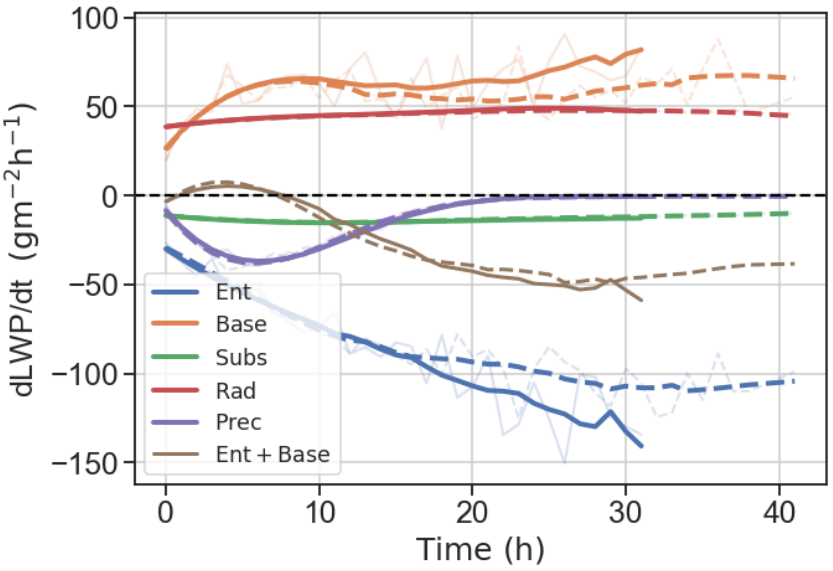

Figure 11: Temporal evolutions of all forcing terms of LWP prognostic equation for CTRL (solid) and FXDLHF (dashed) runs. Plotted are clouds with cloudiness greater than 99%. Lines for Ent_{LWP} and $Base_{LWP}$ are after smoothing, and the unsmoothed values are marked by the semi-transparent lines.

6. Discussion

We have confirmed the indispensable role of LHF in driving the cloud transition during the ASTEX field campaign (Fig 2). Here we discuss two key insights.

6.1. The importance of entrainment efficiency

The entrainment efficiency is crucially important for the LHF-driven cloud transitions, both as external forcing and as feedback. For the ASTEX case, the initial temperature jump across the capping inversion is weak enough (~5.5 K) to cause highly effective entrainment warming, which is the dominant mechanism responsible for the boundary layer decoupling. As the deepening boundary layer erodes into a drier and less stable free atmosphere, evaporative cooling enhances, further increasing the entrainment efficiency. This acts to amplify the preexisting decoupling.

This partially explains the lack of a clear signal of the dependence of boundary layer decoupling on the LHF in observations. We know that the inversion strength of marine boundary layers presents considerable temporal and regional variations (Muhlbauer et al., 2014). The time scale of the lower-tropospheric stability (a proxy for the temperature inversion strength) is on the

order of ~2 days (Eastman et al., 2016), comparable to the time scale of the cloud transition. The inversion strength variations can lead to variations in the entrainment efficiency (Caldwell et al., 2005; Wood, 2012), altering the STBL coupling state to the extent that the signals of LHF are substantially diminished.

6.2. The physical meaning of *Ent* + *Diab*

We found *Ent* + *Diab* is a new model diagnostic that is useful for a physical conceptualization of the boundary layer decoupling. The physical meaning of this diagnostic can be understood from two perspectives. From the perspective of cloud-layer energy balance, radiative cooling tends to balance the warming by entrainment and precipitation. An imbalance toward net warming (i.e. a more positive *Ent* + *Diab*) will cause a downward energy flux at the cloud base, a cooling effect to balance the excessive warming. Such a downward flux of energy near the cloud base is a manifestation of boundary layer decoupling (Bretherton, 1997; Stevens, 2000). Therefore, a larger *Ent* + *Diab* predicts a more decoupled boundary layer. Another perspective is the concept of buoyancy generation and consumption. In a well-mixed boundary layer capped by a Sc deck, the turbulent kinetic energy (TKE) is primarily generated from the radiative cooling near the cloud top. The TKE is consumed by (1) entrainment and precipitation that destabilizes the boundary layer or by (2) viscous dissipation after kinematically mixing the boundary layer fluid. There is a competition between the two. If the consumption by entrainment and precipitation is large, less TKE is available for mixing the boundary layer fluid, which favors the decoupling. Therefore, a larger *Ent* + *Diab* dictates a less energy cost of dissipation per unit of radiatively generated turbulence, corresponding to more likelihood of decoupling.

This diagnostic, however, should not work for decoupling of an STBL drifting over colder water (Zheng and Li, 2019). From the perspective of cloud-layer energy balance, cooling of the underlying surface requires energy supply from above, which must cause downward energy flux somewhere in the boundary layer, leading to the decoupling. From the perspective of buoyancy budgets, the stabilization of the warm-advection flow tends to suppress the TKE, promoting the decoupling. Thus, an additional term that accounts for the strength of the temperature advection should be added to the *Ent* + *Diab* in order to generalize its usage to broader circumstances (e.g. middle latitudes).

7. Conclusion

Surface latent heat flux (LHF) has long been regarded as a crucial controller of stratocumulus (Sc)-to-cumulus (Cu) transition (Krueger et al., 1995; Bretherton and Wyant, 1997; Wyant et al., 1997). A necessary condition for the cloud transition is sea surface warming. As seawater warms up, the LHF must increase, constrained by the Clausius-Clapeyron physics and boundary layer conservation laws. Such an increase in LHF has been argued to drive the two stages of the Sc-to-Cu transition, namely the boundary layer decoupling (first stage) and the breakup of the Sc deck (second stage). This idea, however, is challenged by recent field observations showing no distinct dependence of the boundary layer coupling state on the LHF (Jones et al., 2011; Zhou et al., 2015).

Given the mixed lines of evidence, it is imperative to further investigate the underlying mechanism of LHF influences on cloud transitions.

This study uses LES simulations to isolate the role of increased LHF by conducting a mechanism-denial experiment (FXDLHF) that turns off the LHF adjustment, that is, the LHF is not permitted to increase with the warming sea surface. By comparing it with the control run for a classical Sc-to-Cu transition case from the ASTEX field campaign (CTRL), we can identify how the increase in LHF influences the cloud transitions. The LES modeling results are interpreted in the theoretical frameworks of cloud-layer energy and water balances and a mixed-layer model (Bretherton and Wyant, 1997). The results are summarized as follows:

- The increase in LHF is not a necessary condition for the initiation of boundary layer decoupling. For the ASTEX case, the initial temperature jump across the capping inversion is weak enough (~5.5 K) to cause highly effective entrainment warming, which dominantly drives the decoupling. Such a large influence of the entrainment efficiency might explain the lack of observational evidence for the LHF control on the boundary layer decoupling, given the marked variations of the inversion strength (thereby entrainment efficiency) in time and space.
- The decoupling due to the weak inversion alone, however, cannot sustain without the help of the LHF adjustment. Without an increase of LHF with SST, the boundary layer tends to dry more rapidly due to entrainment, elevating the lifting condensation level (LCL). The growing LCL eventually intercepts with the Sc deck base, recoupling the boundary layer. Energetically speaking, without an increase in LHF to sustain a strong entrainment rate, the entrainment warming can no longer combat the increased diabatic cooling (e.g. increased radiative cooling) as the boundary layer deepens. This ultimately recouples the boundary layer. This result confirms the indispensable role of LHF adjustment in sustaining (although not initiating) the boundary layer decoupling.
- The absence of LHF adjustment tends to delay the breakup of the Sc deck. Without the LHF increase, the Cu convection cannot develop so that the enhanced entrainment drying due to the Cu penetration into the dry inversion can't happen. This helps to sustain the Sc deck longer by ~ 10 hours, even though the surface moisture supply is lower. For the same reason, the transition to Cu regime can never happen without LHF adjustment. This result confirms the theory of "Cu penetrative entrainment" proposed by Wyant et al. (1997).

Lastly, this study develops a new model diagnostic that is useful for a physical conceptualization of the boundary layer decoupling: *Ent* + *Diab*, in which the *Ent* is the entrainment warming and the *Diab* is the diabatic cooling (a combination of radiative cooling and precipitation-induced warming) across the cloud layer, both having the unit of W m^{-2}. This diagnostic can help us to organize our observational and modeling analyses of Sc-to-Cu transitions.

Acknowledgments

This study is supported by the Department of Energy (DOE) Atmospheric System Research program (DE-SC0018996). The SAM model code is available at http://rossby.msrc.sunysb.edu/~marat/SAM.html. We thank Marat Khairoutdinov for maintaining the SAM code. We thank Peter Blossey for helping with setting up the ASTEX case.

Reference:

Abel, S. J., Boutle, I. A., Waite, K., Fox, S., Brown, P. R., Cotton, R., et al. (2017). The role of precipitation in controlling the transition from stratocumulus to cumulus clouds in a Northern Hemisphere cold-air outbreak. *Journal of the Atmospheric Sciences, 74*(7), 2293-2314.

Albrecht, B. A., Bretherton, C. S., Johnson, D., Schubert, W. H., & Frisch, A. S. (1995). The Atlantic stratocumulus transition experiment—ASTEX. *Bulletin of the American Meteorological Society, 76*(6), 889-904.

Bodas-Salcedo, A., Williams, K. D., Ringer, M. A., Beau, I., Cole, J. N., Dufresne, J.-L., et al. (2014). Origins of the solar radiation biases over the Southern Ocean in CFMIP2 models. *Journal of Climate, 27*(1), 41-56.

Bretherton, C. S. (1997). Convection in stratocumulus-topped atmospheric boundary layers. In *The Physics and Parameterization of Moist Atmospheric Convection* (pp. 127-142): Springer.

Bretherton, C. S., & Blossey, P. N. (2014). Low cloud reduction in a greenhouse-warmed climate: Results from Lagrangian LES of a subtropical marine cloudiness transition. *Journal of Advances in Modeling Earth Systems, 6*(1), 91-114.

Bretherton, C. S., Blossey, P. N., & Uchida, J. (2007). Cloud droplet sedimentation, entrainment efficiency, and subtropical stratocumulus albedo. *Geophysical Research Letters, 34*(3).

Bretherton, C. S., Uchida, J., & Blossey, P. N. (2010). Slow manifolds and multiple equilibria in stratocumulus-capped boundary layers. *Journal of Advances in Modeling Earth Systems, 2*(4).

Bretherton, C. S., & Wyant, M. C. (1997). Moisture transport, lower-tropospheric stability, and decoupling of cloud-topped boundary layers. *Journal of the Atmospheric Sciences, 54*(1), 148-167.

Caldwell, P., Bretherton, C. S., & Wood, R. (2005). Mixed-layer budget analysis of the diurnal cycle of entrainment in southeast Pacific stratocumulus. *Journal of the Atmospheric Sciences, 62*(10), 3775-3791.

de Roode, S. R., & Duynkerke, P. G. (1997). Observed Lagrangian transition of stratocumulus into cumulus during ASTEX: Mean state and turbulence structure. *Journal of the Atmospheric Sciences, 54*(17), 2157-2173.

Deardorff, J. (1980). Cloud top entrainment instability. *Journal of the Atmospheric Sciences, 37*(1), 131-147.

Eastman, R., Wood, R., & Bretherton, C. S. (2016). Time scales of clouds and cloud-controlling variables in subtropical stratocumulus from a Lagrangian perspective. *Journal of the Atmospheric Sciences, 73*(8), 3079-3091.

Emanuel, K. A. (1994). *Atmospheric convection*: Oxford University Press on Demand.
Geerts, B. (2019). *Cold-Air Outbreaks in the Marine Boundary Layer Experiment (COMBLE) Science Implementation Plan*. Retrieved from
Hahn, C. J., & Warren, S. G. (2007). *A gridded climatology of clouds over land (1971-96) and ocean (1954-97) from surface observations worldwide*: Oak Ridge National Laboratory, Carbon Dioxide Information Analysis Center.
Hartmann, D. L., Ockert-Bell, M. E., & Michelsen, M. L. (1992). The effect of cloud type on Earth's energy balance: Global analysis. *Journal of Climate, 5*(11), 1281-1304.
Iacono, M. J., Delamere, J. S., Mlawer, E. J., Shephard, M. W., Clough, S. A., & Collins, W. D. (2008). Radiative forcing by long-lived greenhouse gases: Calculations with the AER radiative transfer models. *Journal of Geophysical Research: Atmospheres, 113*(D13).
Jones, C., Bretherton, C., & Leon, D. (2011). Coupled vs. decoupled boundary layers in VOCALS-REx. *Atmospheric Chemistry and Physics, 11*(14), 7143-7153.
kazemirad, M., & Miller, M. A. (2020). Summertime Post-Cold-Frontal Marine Stratocumulus Transition Processes over the Eastern North Atlantic. *Journal of the Atmospheric Sciences, 77*(6), 2011-2037.
Khairoutdinov, M., & Kogan, Y. (2000). A new cloud physics parameterization in a large-eddy simulation model of marine stratocumulus. *Monthly Weather Review, 128*(1), 229-243.
Khairoutdinov, M. F., & Randall, D. A. (2003). Cloud resolving modeling of the ARM summer 1997 IOP: Model formulation, results, uncertainties, and sensitivities. *Journal of the Atmospheric Sciences, 60*(4), 607-625.
Klein, S. A., Hartmann, D. L., & Norris, J. R. (1995). On the relationships among low-cloud structure, sea surface temperature, and atmospheric circulation in the summertime northeast Pacific. *Journal of Climate, 8*(5), 1140-1155.
Krueger, S. K., McLean, G. T., & Fu, Q. (1995). Numerical simulation of the stratus-to-cumulus transition in the subtropical marine boundary layer. Part II: Boundary-layer circulation. *Journal of the Atmospheric Sciences, 52*(16), 2851-2868.
Kuo, H. C., & Schubert, W. H. (1988). Stability of cloud-topped boundary layers. *Quarterly Journal of the Royal Meteorological Society, 114*(482), 887-916.
Lewellen, D., & Lewellen, W. (1998). Large-eddy boundary layer entrainment. *Journal of the Atmospheric Sciences, 55*(16), 2645-2665.
Lilly, D. K. (1968). Models of cloud-topped mixed layers under a strong inversion. *Quarterly Journal of the Royal Meteorological Society, 94*(401), 292-309.
Lloyd, G., Choularton, T. W., Bower, K. N., Gallagher, M. W., Crosier, J., O'Shea, S., et al. (2018). In situ measurements of cloud microphysical and aerosol properties during the break-up of stratocumulus cloud layers in cold air outbreaks over the North Atlantic. *Atmospheric Chemistry and Physics, 18*(23), 17191-17206.
Lock, A. (2009). Factors influencing cloud area at the capping inversion for shallow cumulus clouds. *Quarterly Journal of the Royal Meteorological Society: A journal of the atmospheric sciences, applied meteorology and physical oceanography, 135*(641), 941-952.
McCoy, I. L., Wood, R., & Fletcher, J. K. (2017). Identifying meteorological controls on open and closed mesoscale cellular convection associated with marine cold air outbreaks. *Journal of Geophysical Research: Atmospheres, 122*(21), 11,678-611,702.
Moeng, C.-H., & Rotunno, R. (1990). Vertical-velocity skewness in the buoyancy-driven boundary layer. *Journal of the Atmospheric Sciences, 47*(9), 1149-1162.

Muhlbauer, A., McCoy, I. L., & Wood, R. (2014). Climatology of stratocumulus cloud morphologies: microphysical properties and radiative effects. *Atmospheric Chemistry and Physics, 14*(13), 6695-6716.

Neggers, R., Ackerman, A. S., Angevine, W., Bazile, E., Beau, I., Blossey, P., et al. (2017). Single-column model simulations of subtropical marine boundary-layer cloud transitions under weakening inversions. *Journal of Advances in Modeling Earth Systems, 9*(6), 2385-2412.

Nicholls, S. (1984). The dynamics of stratocumulus: Aircraft observations and comparisons with a mixed layer model. *Quarterly Journal of the Royal Meteorological Society, 110*(466), 783-820.

Nicholls, S., & Leighton, J. (1986). An observational study of the structure of stratiform cloud sheets: Part I. Structure. *Quarterly Journal of the Royal Meteorological Society, 112*(472), 431-460.

Nicholls, S., & Turton, J. (1986). An observational study of the structure of stratiform cloud sheets: Part II. Entrainment. *Quarterly Journal of the Royal Meteorological Society, 112*(472), 461-480.

Randall, D. A. (1980). Conditional instability of the first kind upside-down. *Journal of the Atmospheric Sciences, 37*(1), 125-130.

Riehl, H., Yeh, T., Malkus, J. S., & La Seur, N. E. (1951). The north-east trade of the Pacific Ocean. *Quarterly Journal of the Royal Meteorological Society, 77*(334), 598-626.

Sandu, I., & Stevens, B. (2011). On the factors modulating the stratocumulus to cumulus transitions. *Journal of the Atmospheric Sciences, 68*(9), 1865-1881.

Siems, S. T., & Bretherton, C. S. (1992). A numerical investigation of cloud-top entrainment instability and related experiments. *Quarterly Journal of the Royal Meteorological Society, 118*(507), 787-818.

Siems, S. T., Bretherton, C. S., Baker, M. B., Shy, S., & Breidenthal, R. E. (1990). Buoyancy reversal and cloud-top entrainment instability. *Quarterly Journal of the Royal Meteorological Society, 116*(493), 705-739.

Smolarkiewicz, P. K., & Grabowski, W. W. (1990). The multidimensional positive definite advection transport algorithm: Nonoscillatory option. *Journal of Computational Physics, 86*(2), 355-375.

Stevens, B. (2000). Cloud transitions and decoupling in shear-free stratocumulus-topped boundary layers. *Geophysical Research Letters, 27*(16), 2557-2560.

Stevens, B. (2002). Entrainment in stratocumulus-topped mixed layers. *Quarterly Journal of the Royal Meteorological Society, 128*(586), 2663-2690.

Stevens, B. (2007). On the growth of layers of nonprecipitating cumulus convection. *Journal of the Atmospheric Sciences, 64*(8), 2916-2931.

Stevens, B., Lenschow, D. H., Vali, G., Gerber, H., Bandy, A., Blomquist, B., et al. (2003). Dynamics and chemistry of marine stratocumulus—DYCOMS-II. *Bulletin of the American Meteorological Society, 84*(5), 579-594.

Teixeira, J., Cardoso, S., Bonazzola, M., Cole, J., DelGenio, A., DeMott, C., et al. (2011). Tropical and subtropical cloud transitions in weather and climate prediction models: The GCSS/WGNE Pacific Cross-Section Intercomparison (GPCI). *Journal of Climate, 24*(20), 5223-5256.

Van der Dussen, J., De Roode, S., Ackerman, A. S., Blossey, P. N., Bretherton, C. S., Kurowski, M. J., et al. (2013). The GASS/EUCLIPSE model intercomparison of the stratocumulus

transition as observed during ASTEX: LES results. *Journal of Advances in Modeling Earth Systems, 5*(3), 483-499.
Van der Dussen, J., De Roode, S., & Siebesma, A. (2014). Factors controlling rapid stratocumulus cloud thinning. *Journal of the Atmospheric Sciences, 71*(2), 655-664.
Wood, R. (2012). Stratocumulus clouds. *Monthly Weather Review, 140*(8), 2373-2423.
Wood, R., & Bretherton, C. S. (2006). On the relationship between stratiform low cloud cover and lower-tropospheric stability. *Journal of Climate, 19*(24), 6425-6432.
Wyant, M. C., Bretherton, C. S., Rand, H. A., & Stevens, D. E. (1997). Numerical simulations and a conceptual model of the stratocumulus to trade cumulus transition. *Journal of the Atmospheric Sciences, 54*(1), 168-192.
Xiao, H., Wu, C.-M., & Mechoso, C. R. (2011). Buoyancy reversal, decoupling and the transition from stratocumulus to shallow cumulus topped marine boundary layers. *Climate dynamics, 37*(5-6), 971-984.
Yamaguchi, T., & Randall, D. A. (2008). Large-eddy simulation of evaporatively driven entrainment in cloud-topped mixed layers. *Journal of the Atmospheric Sciences, 65*(5), 1481-1504.
Zheng, Y., & Li, Z. (2019). Episodes of Warm-Air Advection Causing Cloud-Surface Decoupling During the MARCUS. *Journal of Geophysical Research: Atmospheres*.
Zheng, Y., Rosenfeld, D., & Li, Z. (2018). Estimating the decoupling degree of subtropical marine stratocumulus decks from satellite. *Geophysical Research Letters*.
Zheng, Y., Rosenfeld, D., & Li, Z. (2020). A More General Paradigm for Understanding the Decoupling of Stratocumulus-Topped Boundary Layers: The Importance of Horizontal Temperature Advection. *Geophysical Research Letters, 47*(14), e2020GL087697.
Zhou, X., Kollias, P., & Lewis, E. R. (2015). Clouds, precipitation, and marine boundary layer structure during the MAGIC field campaign. *Journal of Climate, 28*(6), 2420-2442.